ACS APPLIED MATERIALS & INTERFACES

Research Article

www.acsami.org

Controlling Mesopore Size and Processability of Transparent Enzyme-Loaded Silica Films for Biosensing Applications

Oswaldo Pérez-Anguiano,[†,‡] Bernard Wenger,[†] Raphaël Pugin,[†] Heinrich Hofmann,[‡] and Emmanuel Scolan*[,†]

[†]Swiss Center for Electronics and Microtechnology (CSEM), Jaquet-Droz 1, CH-2000 Neuchâtel, Switzerland

[‡]Powder Technology Laboratory, École Polytechnique Fédérale de Lausanne, EPFL-STI-IMX-LTP Station 12, CH-1015 Lausanne, Switzerland

Supporting Information

ABSTRACT: Silica-based nanoporous thin films including large mesopores are relevant as enzyme supports for applications in biosensing. The diffusion and immobilization of large biomolecules such as enzymes in such porous films require the presence of large mesopores. Creating such morphologies based on a bottom-up synthesis using colloidal templates is a challenge in view of the combination of desired material properties and the robustness of the casting process for the fabrication of thin films. Here a strategy to reproducibly synthesize transparent porous silica thin films with submicrometer thickness and homogeneously distributed porosity is presented. For this purpose, polystyrene-poly-2-vinylpyridine (PS-P2VP) amphiphilic block copolymers are used as porogenic templates. Low-chain alcohols are employed as both selective solvents for the P2VP blocks and reaction media for silica synthesis. Rheology measurements reveal a strong influence of the block copolymer length on the behavior of PS-P2VP micelles in suspension. The pore distribution and accessibility into the film are controlled by adjusting the silica to block copolymer weight ratio. The solvent choice is shown to control not only the micelle size and the generated pore morphology but also the structural homogeneity of the films. Finally, the suitability of the synthesized films as supports for enzymes is tested using a model enzyme, horseradish peroxidase EC 1.11.1.7. Our approach is innovative, robust, and reproducible and provides a convenient alternative to synthesize large mesopores up to small macropores (20−100 nm) in nanostructured thin films with applications in biosensing and functional coatings.

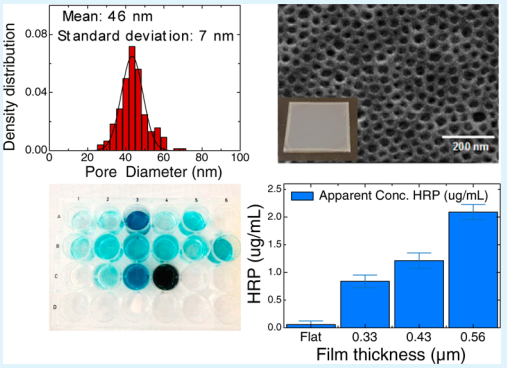

KEYWORDS: *PS-P2VP, amphiphilic block copolymers, large mesopores, thin films, enzyme immobilization, biosensors*

1. INTRODUCTION

Sol−gel-derived thin films with controlled pore structures are materials which find applications as diverse as biosensing, drug delivery, catalysis, or solar cells.[1−7] Whereas their use and versatility for the mentioned applications has been shown, the control of homogeneity and pore size during their synthesis remains a challenge, in particular for the upper end of the mesoporous size range (10−50 nm). Larger pore sizes are desirable whenever these pores are aimed to host relatively large species such as proteins (e.g., enzymes) and to enable their diffusion through the porous medium. The large mesopore size range is therefore of specific relevance to applications in the fields of biosensing, biomedical engineering,[8] or drug delivery.[9] Several methods have been explored to generate pores into sol−gel materials, from bubbling,[10] phase separation,[11−13] emulsion templating,[14] and nanopowder deposition[15] to the embedding of sacrificial organic templates.[16,17] Our goal here is the development of robust procedures to design and master adequate templating approaches to produce mesoporous films in the 20−100 nm size range.

Since the first report on the synthesis of ordered surfactant-templated mesoporous materials,[18] numerous templating strategies to tailor the mesoporosity have been explored.[19−22] Templating materials, e.g., molecular surfactants or block copolymers (BCP), microemulsions,[23] etc., self-organize into large size 3D structures (e.g., micelles). Simultaneously, sol−gel chemistry is used to build a metal oxide framework around them. Using self-assembly principles to template nanostructured metal oxide materials is therefore a highly flexible and efficient strategy to design materials with an enormous variety of structural features.

Pluronic-like block copolymers are based on poly(ethylene oxide) (PEO, hydrophilic block) and poly(propylene oxide) (PPO, hydrophobic block) at different ratios and form stable

Received: December 7, 2014
Accepted: January 9, 2015
Published: January 9, 2015

DOI: 10.1021/am508630c
ACS Appl. Mater. Interfaces 2015, 7, 2960−2971

micelles in solution. Therefore, they have been extensively used as directing agents for the design of porous materials; however, the resulting range of pore sizes is rather limited to small mesopores, usually smaller than 12 nm.[24] This limitation is mainly due to the low HLB (hydrophilic−hydrophobic balance between the PEO and the PPO blocks) and the limited size of the PPO block (70 units) in the available dispersible pluronic block copolymers.

Attempts to form larger pores have been explored. Organic compounds such as 1,3,5-trimethylbenzene (TMB) have been used to increase the micelle size of these polymers, acting as cosurfactants.[25−28] Recently, it has been shown that this method can be optimized by careful selection of the swelling compound, based on its capability to be solubilized within the micelle, achieving a pore size up to 37 nm[2]. Nevertheless, the resulting materials suffer from the lack of homogeneity in porosity, the poor control over the pore shape, and the toxicity issues linked to the use of TMB.

Supercritical CO_2 has been also used as a swelling agent of pluronic-based micelles, avoiding the use of toxic organic compounds. However, this synthesis is time consuming (processing times of several days), is performed in stainless steel chambers at high pressure, and leads to bulk materials. This approach is therefore not adapted to the synthesis of porous films.[29]

Hydrothermal/solvothermal synthesis is yet another commonly reported procedure based on the effect of high pressure and cosolvents to produce large mesopores from 10 to 30 nm;[30−32] however, this approach is commonly only suitable to produce bulk materials, and the pore size reproducibility is poor.[33,34]

Highly amphiphilic block copolymers have now emerged as versatile templating materials for the synthesis of mesoporous structures with controllable pore size, pore symmetry, and diverse chemical compositions. Hydrophilic segments such as PEO, P2VP, or poly(4-vinylpyridine) (P4VP) and hydrophobic segments such as PS, polyisoprene (PI), polybutadiene (PB), and polyacrylonitrile (PAN) are examples of polymer blocks. Recently, Deng et al.[35] reviewed the synthesis of large mesoporous silica and metal oxides using highly amphiphilic block copolymers. According to the authors, chemical compositions, block sequences, molecular weights, and volume fractions of these templating materials can be designed, offering the possibility to be used as templates for the creation of novel mesoporous materials. Moreover, these copolymers can assemble into micelles of larger size compared to the pluronic types and thus are suitable to direct the organization of presynthesized nanocrystals without destruction of the mesostructures. The monitoring of these parameters leads to the synthesis of larger and more stable pores in the range of 10−50 nm with thicker pore walls. Nevertheless, controlling the morphologies in the large mesopore size range remains challenging, mostly because block copolymers with large molecular weights and high dispersibility are needed. Furthermore, methods enabling micelle formation along with the syntheses of metal oxide frameworks are also essential, in particular for the preparation of mesoporous coatings.

Reports about the utilization of amphiphilic templates in the synthesis of porous films mostly rely on evaporation-induced self-assembly (EISA), a common strategy for the nanostructuration of films.[36,37] In EISA, concentrations of block copolymers below their critical micelle concentration (CMC) are used. As the solvent evaporates, the template concentration increases, forming micelles. Templating micelles self-organize with metal oxide precursors into highly ordered and interconnected structures. However, at diluted concentration of polymers, the thickness of the films obtained by this method is limited. Therefore, we propose an innovative approach to produce mesoporous films based on PS-P2VP block copolymer already organized into spherical micelles in a solvent suitable with the sol−gel synthesis of silica oligomers. Thus, the formation of stable and miscible sols of silica precursors and PS-P2VP micelles is the challenge to address.

In this work, we use PS-P2VP block copolymers as templating materials for the synthesis of nanoporous silica films with large mesopores up to small macropores (20−100 nm). More specifically, we established the relationship between the raw material features, the process parameters, and the resulting pore morphology after casting. The raw materials characteristics include BCP block lengths and ratios, solvent, and silica sol precursors. The process parameters comprise the one/two-pot method, the formulation content (e.g., silica to BCP ratio), the spinning speed, and the annealing procedure. In a first attempt to synthesize mesoporous films using PS-P2VP micelles as templates, a one-pot procedure was carried out, mixing molecular silica precursors and micelles at once: silica particles were obtained due to the basicity of the P2VP blocks. Consequently, the conditions to obtain highly homogeneous porosity in submicrometer-thick films with accessible and interconnected pores in a two-step procedure are described. Finally, the assessment of these films as enzyme supports was evaluated following the activity of immobilized HRP in different film structures, proving the suitability of the as-synthesized films in applications such as enzyme-based biosensing.

2. MATERIALS AND METHODS

Materials. PS-P2VP block copolymers were purchased from Polymer Source Inc. (Canada). Any other chemical used in this work was obtained from Sigma-Aldrich and used as received.

Micellar Suspensions. Four milliliter glass vials covered with screw caps and PTFE seals were used. PS-P2VP with different molecular weights were weighed and dissolved in ethanol or 1-butanol at a concentration of 50 mg/mL. Heating at 70 (ethanol) or 95 °C (1-butanol) was necessary to get homogeneous dispersions. For the largest BCP, sonication was needed to induce micellization. The suspensions became translucid when micelles were formed. The micellar suspensions were stable for months.

Sol−Gel Formulation and Film Deposition. Silica was synthesized under acidic catalysis. In a standard procedure, given amounts of tetraethylorthosilicate (TEOS), water, and hydrochloric acid (HCl) 1 M were added to the solvent (ethanol or 1-butanol) at a molar ratio of 1:4:0.02:42, respectively, and stirred at room temperature (20 °C) for 2 h. Micelle suspensions and silica sol aliquots from the previous sol were mixed under magnetic stirring to obtain different suspensions with specific weight ratios of silica-PS-P2VP. The silica−micelle suspension was then spin coated onto borosilicate glass slides (previously cleaned and activated by O_2 plasma treatment) at different speeds for 60 s. Then the samples were heat treated into an air furnace at 550 °C for 20 min.

Micelle Size Measurements. *Atomic Force Microscopy (AFM, Dimension Icon with ScanAsyst, Bruker).* Micellar suspensions of 1−2 mg/mL were prepared from 50 mg/mL suspensions and spin coated onto glass slides. Measurements were performed on these films (tapping mode).

Dynamic Light Scattering (DLS). Dilutions from 50 mg/mL micellar suspensions were prepared and measured by DLS (Zeta PALs, Brookhaven Instruments).

DOI: 10.1021/am508630c
ACS Appl. Mater. Interfaces 2015, 7, 2960−2971

Transmission Electron Microscopy (TEM, Philips/FEI CM12). A drop of 2 mg/mL micellar suspension was poured onto copper grids and dried in a lab hood. Once dried, the grids were placed into a closed vial containing iodine for 30 min at 40 °C.

Rheology. Steady and oscillatory shear rheology was performed using a Physica MCR rheometer (Anton Paar, Germany) with a cone/plate geometry. The mixture was completely enclosed during the measurements, and the solvent trap was filled with the appropriate solvent.

Nanostructure Characterization. Silica porous films were observed by scanning electron microscopy, SEM (XL30 ESEM-FEG, Philips). Thickness values were obtained from cross-section images.

Postfunctionalization. Silica porous films were placed into a desiccator and in an oven for 2 h at 120 °C. (3-Aminopropyl)-triethoxysilane (APTES) (100 μL) was poured in a bottom half of a glass Petri dish equally dried for 2 h. Vacuum was applied until the silane was fully evaporated. After 2 h, the films were taken from the desiccator and placed in an oven at 120 °C for 10 min. No further rinsing was performed.

Estimation of Available Amino Groups. The characterization of postfunctionalized films with APTES was evaluated by a method proposed by Coussot et al.[38] Briefly, the functionalized films were immersed in a staining solution containing an excess of Commassie brilliant blue G (CBB) at acidic pH. After immersion, the films were rinsed with the same solution without dye to remove the excess of nonadsorbed dye. The amine functions are recycled by desorbing the dye with an alkaline buffer. The amount of dye desorbed is quantified colorimetrically; the concentration is obtained using a calibration curve for CBB by comparing the absorbance intensity at λ_{max} = 611 nm.

Enzyme Immobilization and Enzymatic Activity. Films postfunctionalized with APTES were dipped in a solution of glutaraldehyde (Sigma-Aldrich) at 5% (v/v) in a phosphate buffer 0.01 M at pH = 7 for 10 min. Then, they were thoroughly rinsed with deionized water. Glutaraldehyde-modified films were then dipped for 2 h in a horseradish peroxidase EC 1.1.11.7 solution (Sigma-Aldrich) at 10 μg/mL prepared in deionized water. The enzyme-functionalized films are rinsed thoroughly with phosphate buffered saline Tween (PBST, Sigma-Aldrich), phosphate buffered saline (PBS, Sigma-Aldrich), and deionized water and finally dried with compressed air. Enzymatic activity tests are based on the ability of HRP to oxidize 3,3′,5,5′-tetramethylbenzidine (TMB) in the presence of hydrogen peroxide. HRP-loaded films were placed in a 24-multiwell plate, and a given volume of TMB solution (Sigma-Aldrich) was poured into each well containing a film and let to react in darkness for 30 min. Absorbance in the wells was then directly measured at 650 nm using a microplate reader (TECAN infinite M200). Subsequently, the films were removed and sulfuric acid 0.5 M was then added to each well; absorbance is measured at 450 nm after 2 min. A calibration curve is built for known amounts of HRP in solution with TMB, just as described for the enzymatic test. The HRP concentrations calculated for the films using this curve correspond to apparent concentrations of HRP in solution.

3. RESULTS AND DISCUSSION

3.1. Synthesis of Silica sol. The silica sol synthesized under acidic conditions following the molar ratios reported in the experimental section was transparent. Besides, the sol showed good stability after several months of preparation: the solution remained transparent with no evidence of precipitation and gelation. Additionally, the synthesized films using this sol showed the same characteristics independently of the time of preparation. Nevertheless, for comparative studies, the sol was always used 2 h after adding the catalyst (hydrochloric acid).

3.2. Formation and Characterization of Block Copolymer Micelles as Pore Templates. To define the pore structures in the final inorganic films, careful control of the initial porogenic templates was necessary. The aim at this stage was to obtain a stable dispersion of homogeneous spherical micelles of PS-P2VP in a solvent convenient with the silica sol.

Whereas the use of selective solvents for the PS block are widely found in the literature,[39−41] no reports could be found regarding the formation of micelles in selective solvents (aliphatic alcohols) for the P2VP block. This is the first report where a study of micelle formation and characterization is made using selective solvents for the P2VP block. Therefore, we first investigated the relationship between the molecular weight of different BCP, the solvent parameters, and the resulting micelles, focusing on the formation of uniform, spherical micelles suitable to synthesize pores of 20−100 nm in diameter.

The molecular weights of the PS-P2VP block copolymers studied are summarized in Table 1.

Table 1. Overview of the PS-P2VP Block Copolymers Used To Form Micellar Pore Templates

sample	PS block size kg/mol	P2VP block size, kg/mol	P2VP/PS ratio
1	13.5	24	1.77
2	25.5	23.5	0.92
3	28	36	1.28
4	102	97	0.95
5	190	190	1.00

PS-P2VP Solubility in Ethanol and 1-Butanol. According to the available information, PS-P2VP micelles can be prepared in methyl ethyl ketone,[42] toluene,[40] dimethylformamide,[43] tetrahydrofuran,[44] chloroform, methanol, and ethanol, the last two depending on the polymer composition. No information was found regarding the solubilization of PS-P2VP in 1-butanol. From the few options of short-chain aliphatic alcohols used to prepare PS-P2VP micelles, ethanol and 1-butanol were chosen, mainly because they are adequate with the synthesis of silica[45] and less toxic compared to methanol. P2VP is dispersible in low-aliphatic chain alcohols and other polar solvents except water, increasing solubility from shorter to longer aliphatic chain (Table 2). However, polystyrene is not soluble in any of these solvents; hence, ethanol and 1-butanol are selective solvents for the P2VP block. In previous reports dealing with the nanostructuration of materials using PS-P2VP, the followed strategy consisted in either the selection of selective solvents for the PS block[39,40] or the use of good solvents for both blocks, relying on EISA.[43] The explanation about the different solubility behavior and the resulting micelle size of PS-P2VP in ethanol and 1-butanol can be explained first theoretically from the available data of Flory−Huggins interaction parameters for these systems.

Table 2. Solubility Data of P2VP at 25 °C (M_w = 300.8 kg/mol and M_w/M_n = 2.32).[48]

solvent	intrinsic viscosity	Flory−Huggins parameter, χ
1-heptanol	1.22	0.400
1-butanol	1.15	0.445
Ethanol	1.03	0.473

In this work, PS-P2VP of low molecular weights were readily solubilized at room temperature in ethanol forming micelles by magnetic stirring; however, the dispersion and micellization in butanol does not take place as rapidly. Interestingly, at higher

DOI: 10.1021/am508630c
ACS Appl. Mater. Interfaces 2015, 7, 2960−2971

temperature (i.e., 95 °C), 1-butanol promotes a faster solubilization of the block copolymer compared to ethanol. This behavior can be quantified with the Flory–Huggins interaction parameter χ. This parameter measures the interaction in thermal energy units of the polymer chains and the solvent molecules. The critical value of χ for the miscibility of a polymer in a solvent is 0.5 (theta temperature). For values of χ greater than 0.5, the polymer will not be soluble in the solvent.[46] The χ values for P2VP reported by Arichi et al.[47−49] (Table 2) fully support the observations made here; both ethanol and 1-butanol showed values lower than 0.5 values. The value for 1-butanol (0.445) is slightly smaller as compared to ethanol (0.473); in other words, 1-butanol is a better solvent for P2VP than ethanol at room temperature. However, this does not coincide with our observations with ethanol. This result may be explained by the Flory–Huggins parameters of the PS blocks. Flory–Huggins parameter values χ[50] in aliphatic alcohols decrease with increasing temperatures (Table 3) and

Table 3. Flory–Huggins Parameters of Ethanol and 1-Butanol with Respect to Polystyrene[48,50,51]

solvent	average molecular weight (kg/mol), P2VP	Flory–Huggins parameter, χ, PS
ethanol	129.7	1.75, 75 °C
1-butanol	129.7	1.20, 95 °C; 1.44, 75 °C

decreasing with the number of carbons from methanol to hexanol. Therefore, even if polystyrene will not be miscible in 1-butanol at high temperature, smaller PS-P2VP micelle sizes under the experimental conditions used in this work could be expected when 1-butanol is used as a solvent (lower aggregation number) as compared to ethanol.

P2VP is a weak base, and the solubility of P2VP is therefore due to the formation of hydrogen bonding.[52] Arichi et al.[47−49,53] observed higher than expected values for intrinsic viscosity of P2VP in different aliphatic alcohols, which is due to hydrogen bonding between pyridine and alcohol moieties. Larger molecular weight PS-P2VP block copolymers would dissolve faster in 1-butanol at high temperature, where the contribution of the solvent quality of 1-butanol for polystyrene could play a role over the instable hydrogen bonding at higher temperatures.[52]

From this first theoretical description about the solubility of PS-P2VP in aliphatic alcohols and the first qualitative dissolution tests performed over the different PS-P2VP block copolymers listed in Table 1, a clear difference in solubility and viscosities was observed, particularly depending on P2VP/PS length ratio. First, block copolymers with larger PS blocks than the P2VP counterparts were soluble in neither ethanol nor 1-butanol. Second, suspensions of block copolymers with larger P2VP blocks than the PS counterparts were qualitatively more viscous than those with symmetrical blocks. From these observations and as a first step in the characterization of this behavior from micelle suspensions with different block compositions, a rheological study of these systems is proposed.

Rheology of PS-P2VP Micelle Suspensions. As a first investigation toward the preparation of stable silica–micelle suspensions, the rheological properties of the micelle suspensions were studied. These mixed dispersions are then intended to be deposited by spin coating. By spin coating a PS-P2VP dispersion on a flat substrate, a free surface flow is created, where the sample is only in contact with one solid surface formed by the rotating support. Because the upper surface is free, the overall shear rate within the sample is expected to be small.[54,55] In contrast, the rheometry experiments are always performed with the samples confined between *two* solid surfaces. Therefore, the more useful parameter to understand the behavior of the sample is not the shear *rate* but the shear *stress*: It directly influences the force balance of the fluid film, which is determined by an interplay of centrifugal forces created by the spinning disk and the shear stress.

Figure 1 represents the viscosity of samples 1, 2, and 3 as a function of the shear stress. The viscosity of the micelles

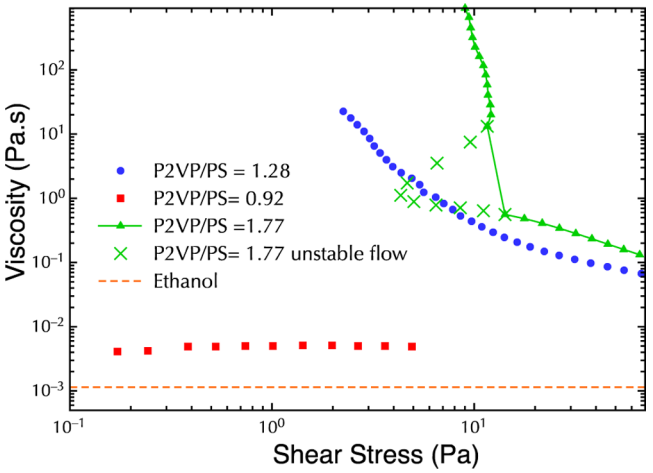

Figure 1. Flow curves from PS-P2VP micellar suspensions in ethanol. Newtonian behavior is observed for symmetrical PS-P2VP (sample 2, squares) block copolymer, whereas asymmetrical blocks (samples 1, triangles; sample 3, circles) show a shear thinning behavior. Unstable flow is shown for highly asymmetrical block copolymer around 10 Pa.

suspension for asymmetric block copolymers (P2VP/PS > 1) was considerably higher compared to other suspensions from almost symmetric block copolymers (P2VP/PS ≈ 1), as shown in the rheology measurements (Figure 1). The sample 2 viscosity effectively does not depend on shear stress (or shear rate). The dispersion viscosity is slightly higher as compared to pure solvent (4 vs 1 mPa·s), but the Newtonian behavior of sample 2 is retained throughout the entire range of shear stresses and rates. However, sample 1 with P2VP/PS of 1.77 shows a shear-thinning behavior with a very high viscosity at low shear rates.

The solvation of P2VP chains in sample 1 not only increases the viscosity of the micelles suspension but also causes formation of a gel-type material with a yield stress and viscoplastic flow behavior (Figure 2). In this figure, the predominantly viscous behavior of sample P2VP/PS = 0.92 is observed, whereas sample P2VP/PS = 1.77 shows a typical gel-like behavior at low strain amplitudes, where the elastic modulus dominates. The linear viscoelastic behavior is limited to small deformations (<1%), with a crossover of the moduli at a deformation around 7%. Above this point the viscous modulus dominates, indicating the transition from a gel-like to a viscous liquid. This drop in the elastic modulus is observed more clearly when plotting the storage (elastic) modulus vs shear stress (inset graph, Figure 2), confirming the point where the gel yields at a stress value around 10 Pa. The critical level of the stress is virtually identical to the value found in the steady

DOI: 10.1021/am508630c
ACS Appl. Mater. Interfaces 2015, 7, 2960−2971

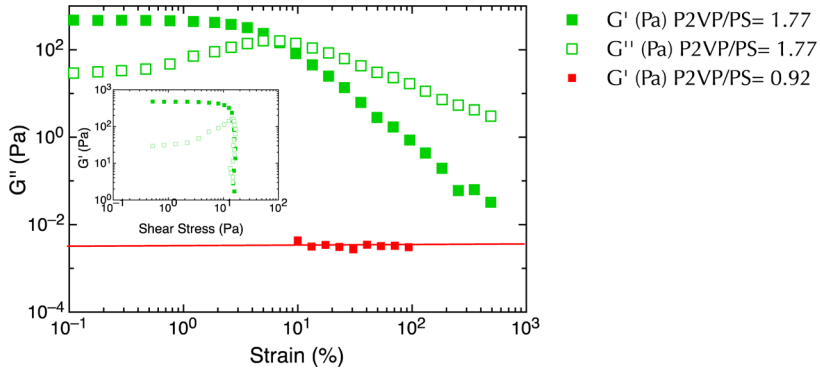

Figure 2. Limiting cases of rheological behavior of the block copolymer templates: Amplitude sweep of samples PS/P2VP = 0.92 (red) and PS/P2VP = 1.77 (green) in ethanol. Sample PS/P2VP = 1.77 behaves as a gel at small strain amplitudes. Sample PS/P2VP = 0.92 shows purely viscous and linear flow behavior. (Inset) Moduli plotted vs shear stress, indicating the linear viscoelastic regime up to stresses around 1 Pa and a dramatic drop in the elastic modulus around 10 Pa, suggesting gel yielding.

Table 4. Summary of Size Measurements for PS-P2VP Block Copolymer Micelles in Ethanol and 1-Butanol by Different Techniques

	DLS (nm)		TEM (nm)		AFM (nm)	
sample	ethanol	butanol	ethanol	butanol	ethanol	butanol
2	81 ± 1	46 ± 1	36 ± 4	26 ± 2	40 ± 6	20 ± 3
4	183 ± 2	142 ± 2	79 ± 10	63 ± 5	99 ± 14	86 ± 9
5	304 ± 4	187 ± 4	136 ± 20	88 ± 11	120 ± 13	87 ± 12

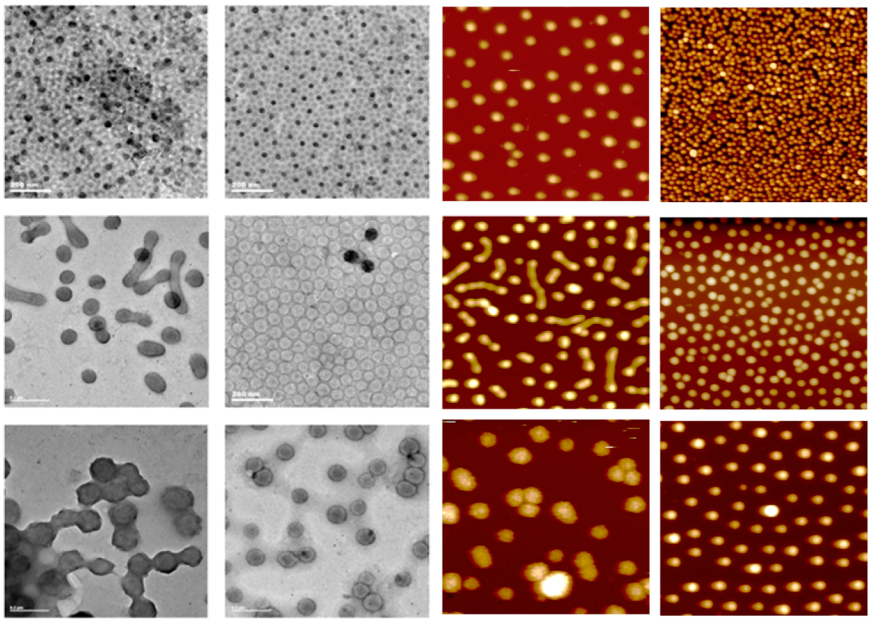

Figure 3. TEM and AFM images of micelles of samples 2, 4, and 5 in descending order prepared in ethanol (left side of each set of images) and 1-butanol (right). Image size of AFM is 2 × 2 μm.

flow curve at the point where the viscosity increases dramatically.

In conclusion, the non-Newtonian rheological behavior of the asymmetric block copolymers with larger P2VP blocks will strongly affect the film casting: even at the highest rotation rate of 6000 rpm (corresponding to an angular velocity of 628.3 rad/s), the block copolymer mixture does not flow during spin coating (test performed, data not shown). This undesirable flow behavior is represented by the onset of viscoplasticity in the rheology data as the asymmetry of the block copolymer increases. In controlled shear rate experiments, where the sample is forced to flow, unstable, nonmonotonic flow behavior is observed[56,57] (Figure 1); in stress-controlled experiments, the sample simply does not flow below a stress of around 10 Pa in the example shown in Figure 2. Therefore, the individual blocks are chosen with identical molecular weights (P2VP/PS = 1.0 ± 0.1) and according to their ability to form micelles with a size range closed to the targeted pore size.

Micelle Size and Morphology. To assess the effect of solvent on the micelle sizes made of symmetrical PS-P2VP blocks, size measurements were performed by DLS on the native micelle dispersions. Additionally, dilutions from these dispersions were

DOI: 10.1021/am508630c
ACS Appl. Mater. Interfaces 2015, 7, 2960−2971

deposited onto copper grids and silicon wafers, and TEM and AFM size measurements, respectively, were performed on the deposited micelles after solvent evaporation. The choice of selective solvent for the P2VP block strongly influenced the micelle size and shape, as shown in Table 4 and Figure 3. Independently of the measurement technique, the micelles of PS-P2VP prepared in ethanol are larger than those prepared in 1-butanol. Additionally, the micelle sizes obtained from DLS measurements showed higher values than those obtained from the other two techniques: the DLS values correspond to the size of solvated micelles in suspension. The values obtained from TEM and AFM reflect the size of the micelles in a dried state.

The micelle size is determined by the solvation capacity for each block, as explained by Antonietti et al.[58] They found that the micelle size of PS-P4VP BCP in selective solvents for polystyrene decreased with increasing solvent capacity for P4VP, the insoluble core. Consistent with these observations, the same tendency is observed for PS-P2VP micelles in selective solvents for P2VP, where micelles sizes are smaller in 1-butanol, which is a better solvent for PS. Lower PS-P2VP micelle sizes are therefore expected when 1-butanol is used as a solvent (lower aggregation number) as compared to ethanol.

In addition, the size of the micelles also increases with the length of the nonsoluble block (PS) as observed in Table 4 and Figure 3. Moreover, rod-like morphologies were observed in both AFM and TEM images for ethanolic micelle suspensions. In contrast, micelles of PS-P2VP prepared in 1-butanol are spherical and highly monodispersed in size.

In Figure 4, the relationship between micelle diameter obtained by TEM and the micelle core given by the PS block

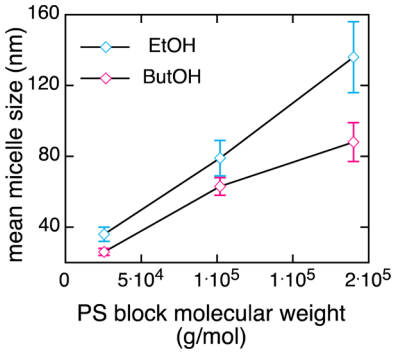

Figure 4. Micelle mean diameter (measured by TEM) as a function of the PS block molecular weight in ethanol and 1-butanol.

molecular weight of symmetrical block copolymer is presented. In this graph, almost a linear relationship is observed between PS block length and micelle sizes for suspensions prepared in ethanol. However, micelles prepared in 1-butanol showed smaller sizes for PS-P2VP of 190 kg/mol. This result is due to the processing temperature difference to produce micelles in ethanol (75 °C) and 1-butanol (95 °C) for sample 5. As shown in Table 3, the Flory–Huggins parameter of 1-butanol for PS at 95 °C is smaller than ethanol at 75 °C, indicating a better solvent capability of 1-butanol at the experimental conditions followed in this study. A better solvent for the core block results in smaller micelle sizes.[58]

Considering the micelle size and shape of PS-P2VP micelles dissolved in ethanol and 1-butanol, a direct consequence in terms of pore sizes and morphologies can be expected after mixing these suspensions with a silica sol. Either option seems suitable to synthesize porous silica films within the aimed range of pore sizes (20–100 nm); however, dispersion of PS-P2VP micelles in 1-butanol are more homogeneous in shape than those prepared in ethanol. For this reason, in the following sections, only results concerning silica films synthesized from micelles prepared in 1-butanol are discussed. However, silica films were synthesized from ethanolic formulations (data not shown), and a qualitative comparison is made in the following sections to emphasize the choice of 1-butanol over ethanol for film synthesis.

3.3. Formulation of Silica- PS-P2VP Templates. A one-pot procedure to synthesize porous silica films was first attempted, resulting in the synthesis of silica particles. A possible explanation for these results lies on the participation of pyridine groups present at the outer surface of PS-P2VP micelles in hydrolysis/condensation reactions with silica species. Previous work by Yamauchi et al.[59−63] demonstrated the interaction of inorganic species from silica and titania with the P2VP block from micelles formed by triblock copolymers PS-P2VP-PEO. In their studies, fully protonated micelles reduced their size measured by DLS after addition of metal alkoxides under acidic catalysis. The reduction in size was associated with the neutralization of fully protonated pyridine groups from the P2VP block, leading to reduced electrostatic repulsion between them. In addition, the formation of a silica wall around P2VP was further characterized by zeta potential measurements, before and after addition of TEOS, revealing a significant decrease from 35 to 5 mV.[60] Taking into account our own findings and the reported observations from similar systems, in this work a two-step procedure was proposed, preparing in parallel a silica sol and a micelle suspension and mixing them before casting to avoid silica particles' formation.

Effect of Silica to Polymer Ratio. The silica moieties in the sol form the solid framework and pore walls in the final films. Therefore, the ratio between the porogenic species (PS-P2VP blocks) and the silica precursors is expected to influence the porous structure of the resulting films.

Ratios of silica to PS-P2VP in weight were varied from 0.33 to 1.33 (Figure 5). The impact of this ratio on the porous structure was assessed by SEM. At low silica content (ratio 0.33), open pores can be observed; nevertheless, their structures are not well defined, and the silica framework is fractured. Due to the lack of silica, micelles have probably merged due to very thin silica walls leading to the formation of larger pores. Images of films prepared with radii from 0.66 to 0.83 show a well-defined nanostructure: open porosity from the surface and no fracture of the silica framework. The pore wall increases when increasing the silica content. Finally, at a ratio of 1.33, the silica content is too large, so that only a few pores are open from the surface. Most of the pores are probably closed.

The image analysis from top view SEM pictures reveals large mesopores and small macropores ranging from 20 to 90 nm in diameter for samples 2, 4, and 5 (Figure 6). This result confirms the choice of block copolymer sizes and the selection of 1-butanol as solvent. Moreover, the pore size distribution is relatively narrow, as the initial micelle size dispersion. The size distribution becomes wider with the molecular weight of the block copolymer (Figure 6).

A deviation from linearity in the pore size diameter can be observed in Figure 7 a, where the micelle size diameters by TEM are compared to the pore sizes observed by SEM. For bigger block copolymer micelles, the variation in size for

DOI: 10.1021/am508630c
ACS Appl. Mater. Interfaces 2015, 7, 2960−2971

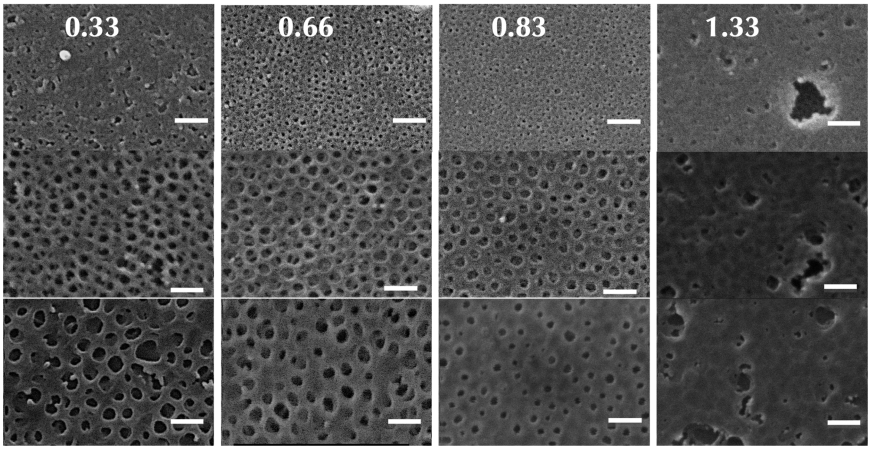

Figure 5. Silica thin film nanostructures obtained from PS-P2VP micelle templating. From top to bottom: samples 2, 4, and 5. Numbers at the top of each column indicate the silica to polymer mass ratio. Scale bar 200 nm.

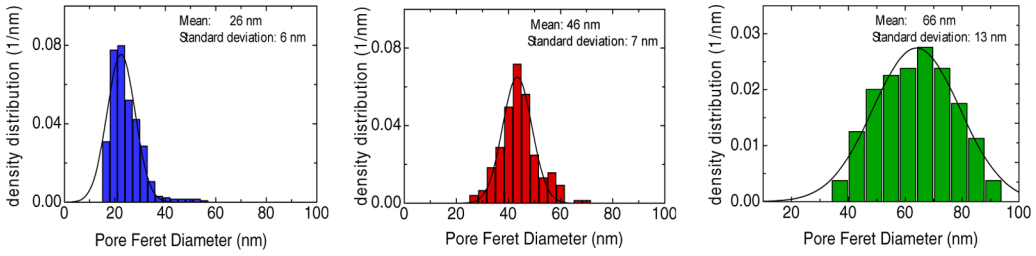

Figure 6. Pore diameter distribution of nanoporous films from image analysis for sample 2 (blue), 4 (red), and 5 (green) at a silica/BCP ratio of 0.66.

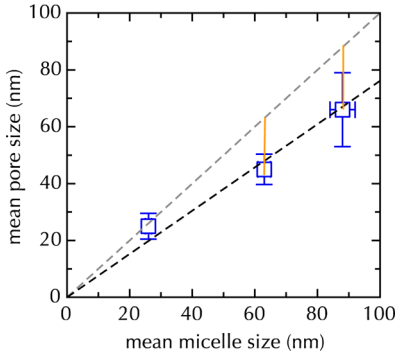

Figure 7. Mean pore diameter as a function of the original micelle size for butanol-based systems measured by TEM. The upper dashed line (slope 1) indicates identical sizes of templating micelles and resulting pores. The lower dashed line (slope 0.76) is a linear fit of the data forced through the origin, fitting the data well above 40 nm but slightly underpredicting the pore size obtained from small micelles. Red segments represent the deviation to the equality dashed line, which has been estimated to be 1.26.

micelles and resulting pores is bigger compared to smaller block copolymers. Considering spherical micelles and assuming equal volumes for the core and the corona due to symmetrical block sizes, the following relation is obtained (Figure 8)

$$V_S = V - V_c = V_c \text{ and then } V = 2V_c$$

where V_s is the volume of the shell (P2VP), V is the total volume of the micelle, and V_c is the volume of the PS core. Defining x as the ratio between the diameters of the full micelle R (core and shell) and of the core r and considering the volume of a sphere

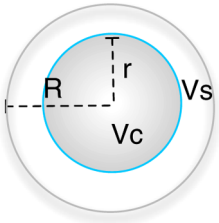

Figure 8. Schematization of a PS-P2VP micelle. R and r correspond to the ratios of the whole micelle and the PS core, respectively, whereas V_c and V_s are the volumes of the PS core and the corona, respectively.

$$x = \frac{R}{r} = \sqrt[3]{2} = 1.26$$

This value is close to the values of the ratio between the micelle size and the pore size calculated from Figure 7 a, namely, 1.36 and 1.33 for samples 4 and 5, respectively. This result confirms that the pore size is mainly defined by the PS core size of the micelles.[58] Indeed, the silica precursors infiltrate the P2VP shell. The additional contribution to this size difference may be attributed to the pore shrinking during the annealing step. For smaller micelles (sample 2), the difference between the micelle size by TEM and the resulting pore size is not as clear as with the larger block copolymers. This might be attributed to a more condensed P2VP shell, which becomes denser as the micelle decreases in diameter. Finally, the expected reduction from linearity in the films depending on the micelle is shown in Figure 7 b. This prediction can be useful to estimate the final pore size depending on the original micelle size.

3.4. Effect of Solvent Evaporation during Spin Coating. Films obtained from butanolic formulations yielded

DOI: 10.1021/am508630c
ACS Appl. Mater. Interfaces 2015, 7, 2960−2971

homogeneously distributed porous films with less thickness variation (striations) along the film compared to ethanolic suspensions (Supporting Information). According to Birnie,[64] several strategies can be applied to reduce striations in complex mixtures (i.e., sol−gel formulations), where water is a key component for hydrolysis−condensation reactions. From his comprehensive study,[64−68] he describes the evaporation process of a sol−gel mixture as a combination of two processes, one concerning the change of concentration of solvents at the surface and another as a cooling effect affecting the surface tension. Surface tension gradients produce a fluid flow from high to low surface tension areas, which progresses causing the thickness variations along the film (striations). As a part of the described strategy, the solvent mixture should contain a solvent with lower vapor pressure and lower surface tension compared to water. Ethanol is not the best choice following this strategy, since it has higher surface tension and vapor pressure than water (Supporting Information). In contrast, 1-butanol does not show this result due to the effect of a low vapor pressure as main solvent during spin coating.

Moreover, the 1-butanol resulting films are highly transparent, i.e., defect free (high homogeneity in thickness and in pore size distribution). By fixing the spinning speed of the spin coater in the 1000−6000 rpm range, the film thickness can be adjusted in the 200−600 nm range. This range is higher than the reported values, usually lower than 100 nm.[69,70]

In conclusion, butanolic sol−gel-derived films were reproducibly produced with very homogeneous porosity and thickness.

3.5. Film Postfunctionalization. To assess the suitability of the silica films to be used as supports for enzyme immobilization, the as-synthesized films were successively postfunctionalized with an aminosilane and glutaraldehyde.

The results presented in the previous sections serve as a guide to select the appropriate block copolymer templates and coating conditions suitable for HRP immobilization. The polymer described as sample 2 (Table 1) is used as a model for the following sections at a silica to polymer ratio of 0.66. This configuration exhibits the smallest pore size and yet the highest surface area. Additionally, the pores from these films are still large enough to allow the enzyme to diffuse. Different films with three different thicknesses are synthesized by adjusting the deposition parameters. A summary of the films used and their characterization after functionalization is shown in Table 5.

Table 5. Description of Samples Used for Enzyme Immobilization

sample	thickness (nm)	Coomassie brilliant blue G concentration (mol/L)	HRP concentration (μg/mL)
reference (flat)		2.76×10^{-06}	0.06
A	330	9.02×10^{-06}	0.84
B	430	1.37×10^{-05}	1.21
C	560	2.46×10^{-05}	2.09

Amino Functionalization of Silica Films. Aminosilane-functionalized porous silica is widely used in bioconjugation techniques for the covalent immobilization of enzymes. In this case, APTES in the vapor phase is used to postmodify the bare silica films with amino functionalities as already reported.[71] This postfunctionalization step is evaluated colorimetrically using CBB (Methods and Materials). This dye binds electrostatically and quantitatively to available protonated primary amino groups in the same way as it is used to quantify proteins.[38] At the acidic pH of the staining solution, the dye is negatively charged while the amino groups are positively charged. This method is simple, reproducible, and nondestructive, allowing the reusability of the films for further enzyme coupling experiments. The spectrum of the dye in the staining solution showed a λ_{max} = 611 nm. From the calibration curve at this wavelength, a value of extinction coefficient of 42 617 L mol^{-1} cm^{-1} nm is found, which is not far from the value of 43 000 L mol^{-1} cm^{-1} reported at 620 nm.[72]

An increase in CBB adsorption is observed by increasing the film thickness. This increase clearly indicates that the higher the thickness, the higher the grafted aminosilane amount on the porous surface. This result confirms that the porosity generated by the PS-P2VP is open and interconnected. A film with a half-micrometer thickness shows 9 times higher dye adsorbed compared to an aminosilane-treated flat glass surface used as a reference (Figure 9).

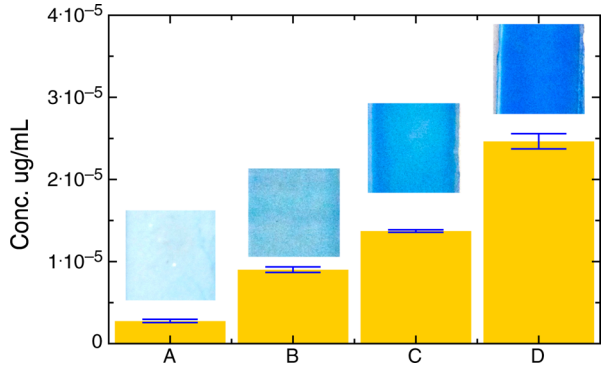

Figure 9. Estimation of available amino groups: Quantification of Coomassie brilliant blue G from amino-functionalized silica films (A and B, Table 4). Amount of adsorbed dye increases with the thickness of the films. (Inset images) CBB adsorption in silica films casted on glass squares of 1 cm^2. The intensity of the blue color is a reflection of the amount of dye adsorbed, which increases with the thickness of the films.

3.6. Enzyme Immobilization and Enzymatic Test. The suitability of the amino-functionalized films to be used as enzyme supports is tested using HRP, a model enzyme. Glutaraldehyde is used as a linker between available amino groups from both the enzyme and the porous silica films previously amino functionalized.[73] This method of immobilization is unspecific, single or multipoint attachment could occur, and loss of enzymatic activity after immobilization is a common and well-known phenomenon.[74] In addition, conformational changes from the enzyme can occur as a consequence of immobilization, independently of the method selected leading to loss of enzymatic activity. Several techniques to characterize these conformational changes have been recently addressed in a review dedicated to enzyme immobilization.[75] However, the advantage of covalent binding is the stability against leaching, which could lead to progressive loss of enzyme over time. For the purpose of this study, the covalent method of immobilization using glutaraldehyde was chosen. The main goal is to demonstrate that the porosity designed in the films is accessible to the enzyme and to prove the suitability of these films as enzyme supports. HRP is a glycoprotein with a diameter of 4−5 nm[76] and with 6 lysine residues available for

DOI: 10.1021/am508630c
ACS Appl. Mater. Interfaces 2015, 7, 2960−2971

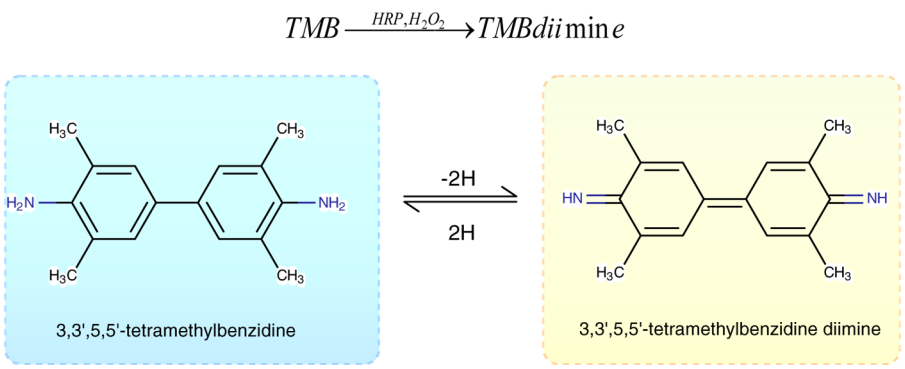

Figure 10. Conversion of TMB into its diimine derivative in an acidic medium.

conjugation.[77] There are several isozymes with isoelectric points ranging from 3 to 9. At pH 7.4 (immobilization buffer) electrostatic interactions can occur between the functionalized silica films and HRP. However, the relatively small size of the enzyme compared to the pore size in the films is expected to allow the transportation of these biomolecules through the pores.

HRP catalyzes the oxidation of redox indicators by H_2O_2, involving the transfer of 2 electrons.[78] In this study, TMB is a chromophore used as the redox indicator, with a characteristic change from colorless (reduced state) to blue (partly oxidized state), and quantitatively measured at the absorbance wavelength λ = 650 nm. Moreover, the fully oxidized TMB is a diimine derivative with a yellow color and with a maximum absorption at 450 nm. The amount of oxidation products was then measured photometrically. For this purpose, the medium was previously acidified to a pH below 1, favoring the equilibrium among all the oxidations species from TMB toward the diimine derivative.[78]

The enzymatic activity of HRP immobilized in porous silica films was monitored through the oxidation of TMB for 30 min (Figures 10 and 11). With no acidification of the medium, the characteristic blue product was formed with a maximum absorbance at 650 nm.[78] The increase in the concentration of oxidized species of TMB (higher absorbance values at 650 nm) was directly related to the increased thickness from the films. Hydrochloric acid 2 M was used to lower the pH below 1. The absorbance measured from porous films loaded with HRP showed in all cases higher values as compared to the flat reference. These absorbance values from porous films are proportional to their thicknesses, as previously observed from the adsorption of CBB (Figure 9).

After addition of hydrochloric acid, the oxidation products from TMB are converted into a diimine derivative with a λ_{max} at 450 nm.[78] A calibration curve is built (see Supporting Information) for known concentrations of HRP in solution with TMB, leading to the calculation of apparent concentration of HRP in the films (Figure 12). These values represent the equivalent concentrations of free enzyme in solution. From Figure 12, the apparent enzymatic activity increases proportionally to the thickness of the film. These values are 14, 20, and 35 times higher than those obtained for a flat surface. These values confirm the previous results about pore accessibility from the CBB adsorption. Despite the low loading

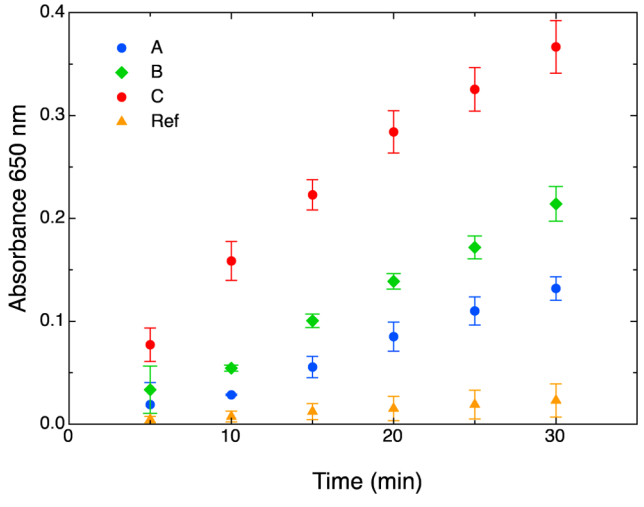

Figure 11. Monitoring of the oxidation of 3,3′,5,5′-tetramethylbenzidine (TMB) from HRP-loaded porous silica films. Higher enzymatic activity is observed from all films evaluated with different thicknesses (red circles, 562 nm; green diamonds, 434 nm; blue circles, 333 nm) as compared to a flat surface used as reference (orange triangles).

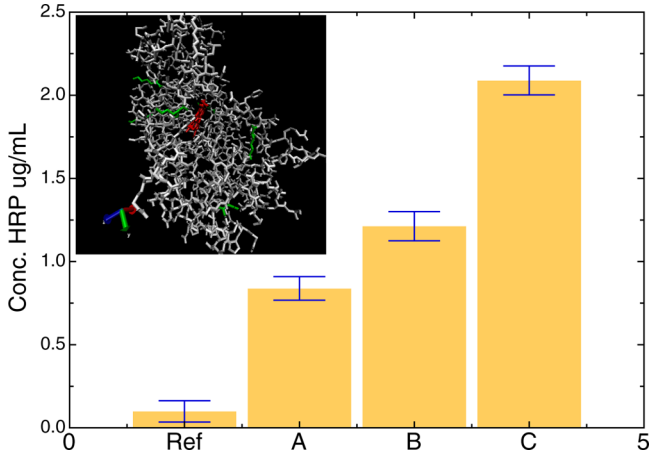

Figure 12. Evaluation of the efficiency of immobilized HRP films in comparison to the free enzyme in solution. For each mesoporous film, the figure shows the activity that can be reached in terms of the equivalent free enzyme concentration. The equivalent concentration increases with the thickness of the films and is much higher for the mesporous films as compared to a flat glass support. The area of the immobilized films is 1 cm^2, and the volume is 1 mL. (Inset) Graphic representation of HRP, pdb 1w4w, using the VMD visualization program from the University of Illinois:[79] green, lysine groups available for conjugation, red, hemoglobin group from the enzyme structure.

DOI: 10.1021/am508630c
ACS Appl. Mater. Interfaces 2015, 7, 2960−2971

concentration (only 10 μg/mL of HRP), the effect of film thickness on the enzymatic activity was observed. In addition, the accessibility of the pores to the enzymes is confirmed.

4. CONCLUSIONS

A highly reproducible method to synthesize transparent nanoporous silica films with pore sizes ranging from large mesopores to small macropores up to 100 nm has been developed. A new method has been developed, based on the entrapment of PS-P2VP micelles preliminary formed in a selective solvent. The influence of the solvent and block copolymer size selection on both the nanostructure and the homogeneity of the film has been demonstrated. In particular, the control of the porous structure was achieved by selecting symmetrical PS-P2VP block copolymers and 1-butanol as the selective solvent for P2VP blocks. Symmetric PS-P2VP-based micellar suspensions behave as Newtonian fluids at the studied concentration, whereas rheology measurements showed that asymmetric block copolymer suspensions at the same concentration form gels, which are unable to be casted as films.

Regarding the film casting, 1-butanol is highlighted as an alternative main solvent to the commonly used ethanol for the synthesis of silica. 1-Butanol-based silica formulations led to even-textured films with homogeneously distributed pores. The silica to polymer ratio is adjusted to each block copolymer formulation to build up an interconnected porous network accessible from the surface of the films, highly transparent, and with thicknesses up to submicrometer scale. Finally, the as-synthesized films were successfully tested as enzyme carriers using HRP as a model. Mesoporous silica films with a submicrometer-scale thickness show an enzymatic activity up to 35 times higher than a functionalized flat support. This reliable method is relevant for the preparation of mesoporous supports for efficient immobilization of large bioentities. These functional mesoporous supports constitute promising patches for the reliable, accurate, and selective detection of analytes in biological media. More specifically, such enzyme-loaded patches will enable the highly sensitive and noninvasive detection of lactate, glucose, and glutamate in body fluids.

■ ASSOCIATED CONTENT

Supporting Information

Experimental data (calibration curves, associated data with enzymatic activity) and photographs from casted silica films. This material is available free of charge via the Internet at http://pubs.acs.org.

■ AUTHOR INFORMATION

Corresponding Author

*E-mail: esn@csem.ch.

Notes

The authors declare no competing financial interest.

■ ACKNOWLEDGMENTS

We gratefully acknowledge the financial support of the NCCR Nanoscale Science from the Swiss National Science Foundation. Prof. Peter Fischer (ETH Zürich) is acknowledged for assistance with preliminary experiments in rheology.

■ REFERENCES

(1) Taguchi, A.; Schüth, F. Ordered Mesoporous Materials in Catalysis. *Microporous Mesoporous Mater.* **2005**, *77* (1), 1−45.
(2) Kruk, M. Access to Ultralarge-Pore Ordered Mesoporous Materials through Selection of Surfactant/Swelling-Agent Micellar Templates. *Acc. Chem. Res.* **2012**, *45* (10), 1678−1687.
(3) Lei, C.; Shin, Y.; Liu, J.; Ackerman, E. J. Entrapping Enzyme in a Functionalized Nanoporous Support. *J. Am. Chem. Soc.* **2002**, *124* (38), 11242−11243.
(4) Hartmann, M. Ordered Mesoporous Materials for Bioadsorption and Biocatalysis. *Chem. Mater.* **2005**, *17* (18), 4577−4593.
(5) Slowing, I. I.; Trewyn, B. G.; Giri, S.; Lin, V. S. Y. Mesoporous Silica Nanoparticles for Drug Delivery and Biosensing Applications. *Adv. Funct. Mater.* **2007**, *17* (8), 1225−1236.
(6) Chen, D.; Huang, F.; Cheng, Y.-B.; Caruso, R. A. Mesoporous Anatase TiO2 Beads with High Surface Areas and Controllable Pore Sizes: A Superior Candidate for High-Performance Dye-Sensitized Solar Cells. *Adv. Mater.* **2009**, *21* (21), 2206−2210.
(7) Lu, Y.; Ganguli, R.; Drewien, C. A.; Anderson, M. T.; Brinker, C. J.; Gong, W.; Guo, Y.; Soyez, H.; Dunn, B.; Huang, M. H.; Zink, J. I. Continuous Formation of Supported Cubic and Hexagonal Mesoporous Films by Sol-Gel Dip-Coating. *Nature* **1997**, *389* (6649), 364−368.
(8) Giri, S.; Trewyn; Brian, G.; Victor SY, Lin Mesoporous Silica Nanomaterial-based Biotechnological and Biomedical Delivery Systems. *Nanomedicine* **2007**, *2* (1), 99−111.
(9) Trewyn, B. G.; Giri, S.; Slowing, I. I.; Lin, V. S. Y. Mesoporous Silica Nanoparticle based Controlled Release, Drug Delivery, and Biosensor systems. *Chem. Commun.* **2007**, *31*, 3236−3245.
(10) Suzuki, K.; Ikari, K.; Imai, H. Synthesis of Mesoporous Silica Foams with Hierarchical trimodal Pore Structures. *J. Mater. Chem.* **2003**, *13* (7), 1812−1816.
(11) Fuertes, M. C.; Soler-Illia, G. J. A. A. Processing of Macroporous Titania Thin Films: From Multiscale Functional Porosity to Nanocrystalline Macroporous TiO_2. *Chem. Mater.* **2006**, *18* (8), 2109−2117.
(12) Fournier, A. C.; Cumming, H.; McGrath, K. M. Assembly of two- and three-Dimensionally Patterned Silicate Materials using Responsive Soft Templates. *Dalton Trans.* **2010**, *39*, 6524−6531.
(13) Triantafillidis, C.; Elsaesser, M. S.; Husing, N. Chemical Phase Separation Strategies Towards Silica Monoliths with Hierarchical Porosity. *Chem. Soc. Rev.* **2013**, *42* (9), 3833−3846.
(14) Nestor, J.; Vílchez, A.; Solans, C.; Esquena, J. Facile Synthesis of Meso/Macroporous Dual Materials with Ordered Mesopores Using Highly Concentrated Emulsions Based on a Cubic Liquid Crystal. *Langmuir* **2012**, *29*, 432−440.
(15) Bowen, P.; Hofmann, H.; Staiger, M.; Steiger, R.; Brugger, P. A.; Peternell, K.; Ttp, Colloidal Processing of Nanoceramic Powders for Porous Ceramic Film Applications. In *Euro Ceramics Vii, Pt 1−3*; Trans Tech Publications Ltd: Zurich-Uetikon, 2002; pp 1977−1980.
(16) Zhao, D.; Yang, P.; Melosh, N.; Feng, J.; Chmelka, B. F.; Stucky, G. D. Continuous Mesoporous Silica Films with Highly Ordered Large Pore Structures. *Adv. Mater.* **1998**, *10* (16), 1380−1385.
(17) Eder, F.; Hüsing, N. Mesoporous Silica Layers with Controllable Porosity and Pore Size. *Appl. Surf. Sci.* **2009**, *256* (3, Supplement), S18−S21.
(18) Kresge, C. T.; Leonowicz, M. E.; Roth, W. J.; Vartuli, J. C.; Beck, J. S. Ordered Mesoporous Molecular Sieves Synthesized by a Liquid-Crystal Template Mechanism. *Nature* **1992**, *359* (6397), 710−712.
(19) Krämer, E.; Förster, S.; Göltner, C.; Antonietti, M. Synthesis of Nanoporous Silica with New Pore Morphologies by Templating the Assemblies of Ionic Block Copolymers. *Langmuir* **1998**, *14* (8), 2027−2031.
(20) Polarz, S.; Antonietti, M. Porous Materials via Nanocasting Procedures: Innovative Materials and Learning about Soft-Matter Organization. *Chem. Commun.* **2002**, *22*, 2593−2604.
(21) Soler-illia, G. J. D.; Sanchez, C.; Lebeau, B.; Patarin, J. Chemical Strategies to Design Textured Materials: from Microporous and Mesoporous Oxides to Nanonetworks and Hierarchical Structures. *Chem. Rev.* **2002**, *102* (11), 4093−4138.

DOI: 10.1021/am508630c
ACS Appl. Mater. Interfaces 2015, 7, 2960−2971

(22) Soler-Illia, G. J. d.; A, A.; Crepaldi, E. L.; Grosso, D.; Sanchez, C. m. Block Copolymer-Templated Mesoporous Oxides. *Curr. Opin. Colloid Interface Sci.* **2003**, *8* (1), 109−126.
(23) Aubery, C.; Solans, C.; Prevost, S.; Gradzielski, M.; Sanchez-Dominguez, M. Microemulsions as Reaction Media for the Synthesis of Mixed Oxide Nanoparticles: Relationships between Microemulsion Structure, Reactivity, and Nanoparticle Characteristics. *Langmuir* **2013**, *29*, 1779−1789.
(24) Deng, Y.; Wei, J.; Sun, Z.; Zhao, D. Large-Pore Ordered Mesoporous Materials Templated from non-Pluronic Amphiphilic Block Copolymers. *Chem. Soc. Rev.* **2013**, *42* (9), 4054−4070.
(25) McGrath, K. M.; Dabbs, D. M.; Yao, N.; Aksay, I. A.; Gruner, S. M. Formation of a Silicate L3 Phase with Continuously Adjustable Pore Sizes. *Science* **1997**, *277* (5325), 552−556.
(26) Feng, P.; Bu, X.; Stucky, G. D.; Pine, D. J. Monolithic Mesoporous Silica Templated by Microemulsion Liquid Crystals. *J. Am. Chem. Soc.* **1999**, *122* (5), 994−995.
(27) Feng, P.; Bu, X.; Pine, D. J. Control of Pore Sizes in Mesoporous Silica Templated by Liquid Crystals in Block Copolymer-Cosurfactant-Water Systems. *Langmuir* **2000**, *16* (12), 5304−5310.
(28) Blin, J. L.; Su, B. L. Tailoring Pore Size of Ordered Mesoporous Silicas Using One or Two Organic Auxiliaries as Expanders. *Langmuir* **2002**, *18* (13), 5303−5308.
(29) Hanrahan, J. P.; Copley, M. P.; Ziegler, K. J.; Spalding, T. R.; Morris, M. A.; Steytler, D. C.; Heenan, R. K.; Schweins, R.; Holmes, J. D. Pore Size Engineering in Mesoporous Silicas Using Supercritical CO_2. *Langmuir* **2005**, *21* (9), 4163−4167.
(30) Matos, J. R.; Kruk, M.; Mercuri, L. P.; Jaroniec, M.; Zhao, L.; Kamiyama, T.; Terasaki, O.; Pinnavaia, T. J.; Liu, Y. Ordered Mesoporous Silica with Large Cage-Like Pores: Structural Identification and Pore Connectivity Design by Controlling the Synthesis Temperature and Time. *J. Am. Chem. Soc.* **2002**, *125* (3), 821−829.
(31) Zhao, D. Y.; Feng, J. L.; Huo, Q. S.; Melosh, N.; Fredrickson, G. H.; Chmelka, B. F.; Stucky, G. D. Triblock Copolymer Syntheses of Mesoporous Silica with Periodic 50 to 300 angstrom Pores. *Science* **1998**, *279* (5350), 548−552.
(32) Kim, T.-W.; Ryoo, R.; Kruk, M.; Gierszal, K. P.; Jaroniec, M.; Kamiya, S.; Terasaki, O. Tailoring the Pore Structure of SBA-16 Silica Molecular Sieve through the Use of Copolymer Blends and Control of Synthesis Temperature and Time. *J. Phys. Chem. B* **2004**, *108* (31), 11480−11489.
(33) Sayari, A.; Liu, P.; Kruk, M.; Jaroniec, M. Characterization of Large-Pore MCM-41 Molecular Sieves Obtained via Hydrothermal Restructuring. *Chem. Mater.* **1997**, *9* (11), 2499−2506.
(34) Kolen'ko, Y. V.; Maximov, V. D.; Garshev, A. V.; Meskin, P. E.; Oleynikov, N. N.; Churagulov, B. R. Hydrothermal Synthesis of Nanocrystalline and Mesoporous Titania from Aqueous Complex Titanyl Oxalate Acid Solutions. *Chem. Phys. Lett.* **2004**, *388* (4−6), 411−415.
(35) Deng, Y.; Wei, J.; Sun, Z.; Zhao, D. Large-Pore Ordered Mesoporous Materials Templated from non-Pluronic Amphiphilic Block Copolymers. *Chem. Soc. Rev.* **2013**, *42* (9), 4054−4070.
(36) Bass, J. D.; Belamie, E.; Grosso, D.; Boissiere, C.; Coradin, T.; Sanchez, C. Nanostructuration of Titania Films Prepared by Self-Assembly to Affect Cell Adhesion. *J. Biomed. Mater. Res., Part A* **2010**, *93A* (1), 96−106.
(37) Sanchez, C.; Boissiere, C.; Grosso, D.; Laberty, C.; Nicole, L. Design, Synthesis, and Properties of Inorganic and Hybrid Thin Films Having Periodically Organized Nanoporosity. *Chem. Mater.* **2008**, *20* (3), 682−737.
(38) Coussot, G.; Perrin, C.; Moreau, T.; Dobrijevic, M.; Postollec, A.; Vandenabeele-Trambouze, O. A Rapid and Reversible Colorimetric Assay for the Characterization of Aminated Solid Surfaces. *Anal. Bioanal. Chem.* **2011**, *399* (3), 1061−1069.
(39) Lu, J. Q.; Yi, S. S. Uniformly Sized Gold Nanoparticles Derived from PS-b-P2VP Block Copolymer Templates for the Controllable Synthesis of Si Nanowires. *Langmuir* **2006**, *22* (9), 3951−3954.
(40) Krishnamoorthy, S.; Pugin, R.; Brugger, J.; Heinzelmann, H.; Hoogerwerf, A. C.; Hinderling, C. Block Copolymer Micelles as Switchable Templates for Nanofabrication. *Langmuir* **2006**, *22* (8), 3450−3452.
(41) Frömsdorf, A.; Kornowski, A.; Pütter, S.; Stillrich, H.; Lee, L.-T. Highly Ordered Nanostructured Surfaces Obtained with Silica-Filled Diblock-Copolymer Micelles as Templates. *Small* **2007**, *3* (5), 880−889.
(42) Cho, Y.-H.; Yang, J.-E.; Lee, J.-S. Size Control of Polymeric Nanoparticles from Polystyrene-b-poly(2-vVinylpyridine). *Mater. Sci. Eng., Proc. Conf.* **2004**, *24* (1−2), 293−295.
(43) Shin, W.-J.; Kim, J.-Y.; Cho, G.; Lee, J.-S. Highly Selective Incorporation of SiO2 Nanoparticles in PS-b-P2VP Block Copolymers by Quaternization. *J. Mater. Chem.* **2009**, *19* (39), 7322−7325.
(44) Yang, C. C.; Wu, P. T.; Chen, W. C.; Chen, H. L. Low Dielectric Constant Nanoporous Poly(methyl silsesquioxane) using Poly (Styrene-block-2-Vinylpyridine) as a Template. *Polymer* **2004**, *45* (16), 5691−5702.
(45) Bernards, T. N. M.; Janssen, M. J. C. H.; van Bommel, M. J. Influence of Butanol on the Hydrolysis-Condensation Behaviour of TEOS. *J. Non-Cryst. Solids* **1994**, *168* (3), 201−212.
(46) Danner, R. P. a., Martin, S. *Handbook of Polymer Solution Thermodynamics*; American Institute of Chemical Engineers: New York, 1993.
(47) Arichi, S. Studies of Poly-2-vinylpyridine. III. Intrinsic Viscosity and Molecular Weight. *Bull. Chem. Soc. Jpn.* **1966**, *39* (3), 439−446.
(48) Arichi, S.; Matsuura, H.; Tanimoto, Y.; Murata, H. Studies of Poly-2-vinylpyridine. II. Solubilities in Various Solvents. *Bull. Chem. Soc. Jpn.* **1966**, *39* (3), 434−439.
(49) Arichi, S.; Mitsuta, S.; Sakamoto, N.; Murata, H. Studies of Poly-2-vinylpyridine. I. Suspension Polymerization and Molecular Weight Distribution. *Bull. Chem. Soc. Jpn.* **1966**, *39* (3), 428−434.
(50) Bernardo, G.; Vesely, D. Equilibrium Solubility of Alcohols in Polystyrene Attained by Controlled Diffusion. *Eur. Polym. J.* **2007**, *43* (3), 938−948.
(51) Brandrup, J. I., E.H. Grulke, E. A. *Polymer Handbook*. 4th ed.; John Wiley & Sons, Inc.: New York, 1999; Vol. *2*.
(52) Dubin, P. L. A Polymer-Solution "thermometer": A demonstration of the Thermodynamic consequences of Specific Polymer-Solvent Interactions. *J. Chem. Educ.* **1981**, *58* (11), 866.
(53) Arichi, S.; Yoshida, M.; Ogawa, Y. The Specific Refractive Index Increment and the Partial Specific Volume of Atactic Poly (2-vinylpyridine). *Bull. Chem. Soc. Jpn.* **1975**, *48* (5), 1417−1422.
(54) Lawrence, C. J.; Zhou, W. Spin Coating of non-Newtonian fluids. *J. Non-Newtonian Fluid Mech.* **1991**, *39* (2), 137−187.
(55) Burgess, S. L.; Wilson, S. D. R. Spin-Coating of a Viscoplastic Material. *Phys. Fluids* **1996**, *8* (9), 2291−2297.
(56) Fischer, P. Time Dependent Flow in Equimolar Micellar Solutions: Transient Behavior of the Shear Stress and First Normal Stress Difference in Shear Induced Structures Coupled with Flow Instabilities. *Rheol. Acta* **2000**, *39* (3), 234−240.
(57) Herle, V.; Fischer, P.; Windhab, E. J. Stress Driven Shear Bands and the Effect of Confinement on their Structures - A Rheological, Flow Visualization and Rheo-SALS Study. *Langmuir* **2005**, *21* (20), 9051−9057.
(58) Antonietti, M.; Heinz, S.; Schmidt, M.; Rosenauer, C. Determination of the Micelle Architecture of Polystyrene/Poly(4-vinylpyridine) Block Copolymers in Dilute Solution. *Macromolecules* **1994**, *27* (12), 3276−3281.
(59) Li, Y.; Bastakoti, B. P.; Imura, M.; Hwang, S. M.; Sun, Z.; Kim, J. H.; Dou, S. X.; Yamauchi, Y. Synthesis of Mesoporous TiO_2/SiO_2 Hybrid Films as an Efficient Photocatalyst by Polymeric Micelle Assembly. *Chem.—Eur. J.* **2014**, *20* (20), 6027−6032.
(60) Bastakoti, B. P.; Li, Y.; Miyamoto, N.; Sanchez-Ballester, N. M.; Abe, H.; Ye, J.; Srinivasu, P.; Yamauchi, Y. Polymeric Micelle Assembly for the Direct Synthesis of Functionalized Mesoporous Silica with Fully Accessible Pt Nanoparticles Toward an Improved CO Oxidation Reaction. *Chem. Commun.* **2014**, *50* (65), 9101−9104.
(61) Li, Y.; Bastakoti, B. P.; Imura, M.; Suzuki, N.; Jiang, X.; Ohki, S.; Deguchi, K.; Suzuki, M.; Arai, S.; Yamauchi, Y. Synthesis of a Large-Sized Mesoporous Phosphosilicate Thin Film through Evaporation-

DOI: 10.1021/am508630c
ACS Appl. Mater. Interfaces 2015, 7, 2960−2971

Induced Polymeric Micelle Assembly. *Chem. Asian J.* **2015**, *10* (1), 183−187.
(62) Bastakoti, B. P.; Salunkhe, R. R.; Ye, J.; Yamauchi, Y. Direct Synthesis of a Mesoporous TiO_2-RuO_2 Composite through Evaporation-Induced Polymeric Micelle Assembly. *Phys. Chem. Chem. Phys.* **2014**, *16* (22), 10425−10428.
(63) Bastakoti, B. P.; Torad, N. L.; Yamauchi, Y. Polymeric Micelle Assembly for the Direct Synthesis of Platinum-Decorated Mesoporous TiO2 toward Highly Selective Sensing of Acetaldehyde. *ACS Appl. Mater. Interfaces* **2013**, *6* (2), 854−860.
(64) Birnie, D. P. Rational Solvent Selection Strategies to Combat Striation Formation during Spin Coating of Thin Films. *J. Mater. Res.* **2001**, *16* (04), 1145−1154.
(65) Birnie, D. P., III; Kaz, D.; Taylor, D. Surface Tension Evolution During Early Stages of Drying of Sol-Gel Coatings. *J. Sol-Gel Sci. Technol.* **2009**, *49* (2), 233−237.
(66) Birnie, D. P.; Manley, M. Combined Flow and Evaporation of Fluid on a Spinning Disk. *Phys. Fluids* **1997**, *9* (4), 870−875.
(67) Haas, D. E.; Birnie, D. P., III Evaluation of Thermocapillary Driving Forces in the Development of Striations during the Spin Coating Process. *J. Mater. Sci.* **2002**, *37* (10), 2109−2116.
(68) Taylor, D. J.; Birnie, D. P. A Case Study in Striation Prevention by Targeted Formulation Adjustment: Aluminum Titanate Sol-Gel Coatings. *Chem. Mater.* **2002**, *14* (4), 1488−1492.
(69) Nagarajan, S.; Li, M.; Pai, R. A.; Bosworth, J. K.; Busch, P.; Smilgies, D. M.; Ober, C. K.; Russell, T. P.; Watkins, J. J. An Efficient Route to Mesoporous Silica Films with Perpendicular Nanochannels. *Adv. Mater.* **2008**, *20* (2), 246−251.
(70) Faustini, M.; Nicole, L.; Boissière, C.; Innocenzi, P.; Sanchez, C.; Grosso, D. Hydrophobic, Antireflective, Self-Cleaning, and Antifogging Sol−Gel Coatings: An Example of Multifunctional Nanostructured Materials for Photovoltaic Cells. *Chem. Mater.* **2010**, *22* (15), 4406−4413.
(71) Juvaste, H.; Iiskola, E. I.; Pakkanen, T. T. Preparation of New Modified Catalyst Carriers. *J. Mol. Catal. A: Chem.* **1999**, *150* (1−2), 1−9.
(72) Chial, H. J.; Thompson, H. B.; Splittgerber, A. G. A Spectral Study of the Charge Forms of Coomassie Blue G. *Anal. Biochem.* **1993**, *209* (2), 258−266.
(73) Hermanson, G. T. In *Bioconjugate Techniques (Second ed.)*, Hermanson, G. T., Ed.; Academic Press: New York, 2008; Chapter 4 (Homobifunctional Crosslinkers), pp 234−275.
(74) Trevan, M. D., Enzyme Immobilization by Covalent Bonding. In *New Protein Techniques*; Walker, J., Ed.; Humana Press: Clifton, New Jersey, 1988; Chapter 37, pp 495−510.
(75) Secundo, F. Conformational Changes of Enzymes upon Immobilisation. *Chem. Soc. Rev.* **2013**, *42* (15), 6250−6261.
(76) Sun, J.; Zhou, H.; Jin, Y.; Wang, M.; Li, Y.; Gu, N. Magnetically Enhanced Dielectrophoretic Assembly of Horseradish Peroxidase Molecules: Chaining and Molecular Monolayers. *ChemPhysChem* **2008**, *9* (13), 1847−1850.
(77) Zhao, Z.; Tian, J.; Wu, Z.; Liu, J.; Zhao, D.; Shen, W.; He, L. Enhancing Enzymatic Stability of Bioactive Papers by Implanting Enzyme-Immobilized Mesoporous Silica Nanorods into Paper. *J. Mater. Chem. B* **2013**, *1* (37), 4719−4722.
(78) Bally, R. W. a.; T. C, J. G. Some Aspects of the Chromogen 3,3′,5,5′-Tetramethylbenzidine as Hydrogen Donor in a Horseradish Peroxidase Assay. *J. Clin. Chem. Clin. Biochem.* **1989**, *27*, 791−796.
(79) Humphrey, W.; Dalke, A.; Schulten, K. VMD: Visual Molecular Dynamics. *J. Mol. Graphics* **1996**, *14* (1), 33−38.

DOI: 10.1021/am508630c
ACS Appl. Mater. Interfaces 2015, 7, 2960−2971